

Blocking transition of SrTiO₃ surface dipoles in MoS₂/SrTiO₃ field effect transistors with counterclockwise hysteresis

Santu Prasad Jana, S Sreesanker, Suraina Gupta, and Anjan K. Gupta
Department of Physics, Indian Institute of Technology Kanpur, Kanpur 208016, India
 (Dated: October 22, 2024)

A counterclockwise hysteresis is observed at room temperature in the transfer characteristics of SrTiO₃ (STO) gated MoS₂ field effect transistor (FET) and attributed to bistable dipoles on the STO surface. The hysteresis is expectedly found to increase with increasing range, as well as decreasing rate, of the gate-voltage sweep. The hysteresis peaks near 350 K while the transconductance rises with rising temperature above the room temperature. This is attributed to a blocking transition arising from an interplay of thermal energy and an energy-barrier that separates the two dipole states. The dipoles are discussed in terms of the displacement of the puckered oxygen ions at the STO surface. Finally, the blocking enables a control on the threshold gate-voltage of the FET over a wide range at low temperature which demonstrates it as a heat assisted memory device.

INTRODUCTION

Atomically thin semiconducting transition metal dichalcogenides (TMDs) [1] are advantageous when integrated into field effect transistors (FETs). Molybdenum disulfide (MoS₂) is a convenient TMD for probing and optimizing such two dimensional (2D) material devices due to its natural abundance and environmental stability. It also offers mechanical flexibility, high transparency, layer-thickness-dependent bandgap [2, 3], higher mobility values than organic semiconductor FETs and excellent electrostatic gate control. Many electronic [3–6] and optoelectronic [3, 7–9] applications have been successfully demonstrated using few layer MoS₂.

Interface-traps between a 2D semiconductor and dielectric gate or the substrate, in a FET, pose a challenge for 2D material electronic devices as they lead to a clockwise (or positive) hysteresis in the transfer characteristics and reduced mobility which limit the devices' potential [10–14]. The hysteresis has also sparked interest in the potential applications of MoS₂ in thermally assisted non-volatile memory devices [14]. In this context, integrating MoS₂ with a ferroelectric (FE) substrate, such as Lead-zirconate-titanate (PZT), is promising as a FE offers higher polarization induced charge density than a dielectric substrate. A PZT substrate in MoS₂ FETs often shows the expected counterclockwise (or negative) hysteresis [15–17]. However, an unwanted “anti-hysteresis”, similar to that due to traps, has also been reported [18–20] due to accumulation of charges at the polar ferroelectric surface that leads to polarization screening.

High dielectric constant gate materials, such as SrTiO₃ (STO) [21], are also of interest as they help suppress long-range charged impurity scattering, thereby enhancing the carrier mobility. A number of studies have investigated transport in graphene on STO thin films [22, 23] and STO bulk substrates [24–27] over a wide temperature range to examine the effects of its large and tunable dielectric constant. Although STO is widely recognized as a paraelectric [28–32] material, a rare ferroelectric-

like counter-clockwise hysteresis [25] has been reported in graphene-STO FETs and attributed to puckered oxygen ions on the STO surface together with the more common clockwise hysteresis [22, 23, 26, 27].

In this paper, we report on ferroelectric-like counterclockwise hysteresis in MoS₂ FET with STO single-crystal substrate as back-gate. The hysteresis increases with increasing sweep-range and with decreasing sweep-rate of the gate voltage. With temperature increasing above room temperature, the transconductance monotonically rises but the hysteresis peaks near 350 K. This is attributed to the bistability of the puckered oxygen ions on the STO surface enabling two dipole states with gate electric field providing a bias between the two states. The hysteresis peak is discussed in terms of the blocking transition of the surface dipoles. The blocking is used to program the dipoles' state through gate-cooling to control the FET's threshold voltage at low temperatures.

EXPERIMENTAL DETAILS

Acetone/IPA cleaned 0.5 mm thick single side polished STO substrate (from Crystal GmbH) with (001) orientation is used as gate dielectric. A 50 nm thick gold film deposited by thermal evaporation on the rough surface of STO substrate, serves as the backgate electrode. Multi-layer MoS₂ flake is mechanically exfoliated from natural bulk crystal (from SPI) and transferred on the STO by a dry transfer method [33] using PDMS film (Gel film from Gel Pak) and an XYZ micromanipulator attached with an optical microscope. To increase the adhesion between the MoS₂ flake and the STO substrate, hexamethyldisilane (HMDS) was spin-coated at 2000 rpm for 45 s prior to the MoS₂ transfer on the polished side of the STO substrate. This also helps in eliminating the effect of interface traps [34]. Nevertheless, the blocking transition is found to be unaffected by the presence of the HMDS layer or by the roughness of the STO surface, see Appendix.

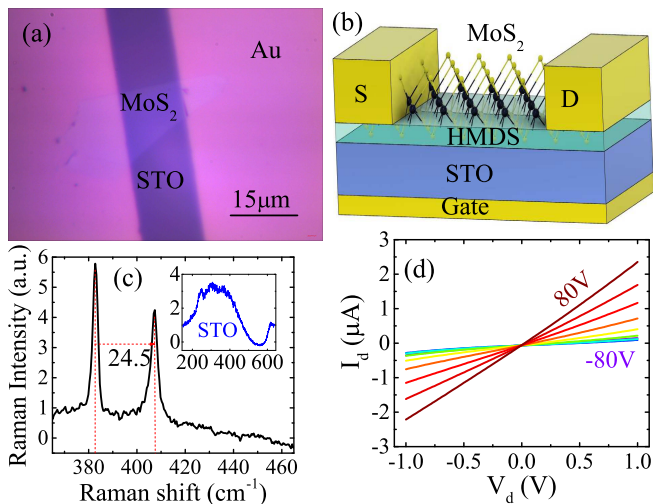


FIG. 1: (a) Optical image of multi-layer MoS₂ on HMDS coated STO substrate with gold contacts. (b) shows a schematic illustration of the FET device with source drain and gate electrodes of gold. (c) Raman spectrum of exfoliated multi-layer MoS₂ on STO. The inset shows the Raman spectrum of the bare STO substrate. (d) I_d versus V_d curves of the device at room temperature at different V_g values between -80 and 80 V separated by 20 V.

Source and drain contacts of gold are made using mechanical masking with a 15 μm diameter tungsten wire by aligning the MoS₂ flake underneath the wire with the help of an optical microscope, followed by 50-nm-thick gold film deposition by thermal evaporation. Fig. 1(a) shows the optical image of fabricated Multi-layer MoS₂/STO FET with gold contacts. Use of mechanical masking helps avoid the organic lithography resists which can leave residue on MoS₂. Fig. 1(b) shows the schematic of the device with source-drain contacts on MoS₂ as well as gate electrode of Au. Fig. 1(c) shows the Raman spectra of the MoS₂ with a smooth background coming from the STO substrate. The two characteristic Raman peaks of MoS₂, E_{2g}^1 and A_{1g} , are separated by 24.5 cm⁻¹ which corresponds to multilayer MoS₂ as reported in the literature [35, 36]. The inset of Fig. 1(c) shows the Raman spectra of the bare STO substrate with the second-order vibrational modes of STO [37].

The two-probe electrical transport measurements used a drain-source voltage bias V_d controlled by a data acquisition card. The drain current I_d is measured through the voltage across a small bias resistor in series with the channel and by using a differential voltage amplifier. A 10 kΩ series resistor was connected to the gate voltage V_g supply to protect it and other electronics in case of gate failure. The gate supply was controlled by the data acquisition card using a LabView program. The linear two-probe current-voltage characteristics, illustrated in Fig. 1(d) at different V_g values, confirmed the Ohmic contacts. All electrical measurements down to 80 K were

conducted in a homemade vacuum cryostat with a heater for temperature control. The cryostat was pumped by a turbomolecular pump to better than 10⁻⁴ mbar vacuum which improves further when the cryostat is immersed in liquid nitrogen for cooling.

BLOCKING TRANSITION IN BISTABLE SYSTEM

Here, basic physics of blocking transition, relevant for the studied MoS₂/STO FET device, is reviewed briefly. A bistable system consists of two metastable minimum energy states that are separated by an energy barrier of height Δ_0 , see the free energy plot in Fig. 2(a). A biasing energy E_B , enabled by the gate electric field in the FET, makes the heights of the barrier, as seen from the two minima, unequal, *i.e.* $\Delta_0 \pm E_B$. This leads to more thermally activated transitions from the shallow to the deep minimum than the other way and larger equilibrium population in the deep minimum. Note that we are assuming an ensemble of identical such two state systems. A superparamagnetic nanoparticle is an example of such a bistable system, see suppl-info of ref-[13], which exhibits blocking transition. Here, the barrier arises from the magnetic anisotropy energy and the biasing energy is dictated by the applied magnetic field.

At a given temperature T , the transition rates $\tau_{1,2}^{-1}$ between the two minima are given by $\tau_0^{-1} \exp[-(\Delta_0 \pm E_B)/k_B T]$ with τ_0^{-1} as the attempt rate. These rates are monotonically rising with increasing temperature and imply a rise in system's response with temperature for a fixed bias. The interplay of the transition rate and the rate τ_m^{-1} of the experimentally controlled bias-energy change, and the history, dictate the evolution of the population distribution in the two minima. The transition rates $\tau_{1,2}^{-1}$ are steeply rising functions of temperature and these will match with τ_m^{-1} at some temperature T_B given by, $T_B \approx \Delta_0/[k_B \ln(\tau_m/\tau_0)]$. Note that a very small bias, *i.e.* $E_b \ll \Delta_0$, is assumed so that it does not make any of the minima disappear and the transition rates are predominantly dictated by Δ_0 .

Below T_B the system's response to the change in bias will be small while above T_B the system will show a large response. The crossover that occurs at T_B is called the Blocking transition. Further, when the bias is swept at a constant rate between two opposite extreme biases $\pm E_{b0}$ over a time τ_m , the population-difference between the two minima at zero bias during the two sweep directions can be written as

$$\Delta p \propto \left[1 - \exp \left\{ -\frac{\tau_m}{2\tau_0} \exp \left(-\frac{\Delta_0 - aE_{b0}}{k_B T} \right) \right\} \right] \times \exp \left\{ -\frac{\tau_m}{2\tau_0} \exp \left(-\frac{\Delta_0 + bE_{b0}}{k_B T} \right) \right\}. \quad (1)$$

Here, a and b are empirical constants less than one and depend on the magnitude of the bias. This expression has been elaborated in the suppl-info of ref-13 for a superparamagnetic system.

RESULTS AND ANALYSIS

Figure 2(b) shows the room temperature $I_d - V_g$ characteristics of multi-layer MoS₂-STO FET at $V_d = 1$ V. The forward V_g sweep curve is seen to be shifted towards right while the reverse-sweep curve is shifted towards left. This amounts to a counterclockwise hysteresis as opposed to the clockwise hysteresis in MoS₂/SiO₂ FETs [13] due to the interface traps. In these MoS₂-STO FETs, the threshold voltage V_{th} is not seen in all the $I_d - V_g$ curves over used V_g range. Thus, we quantify the hysteresis by the apparent relative V_g shift, *i.e.* ΔV_h , between the two sweep directions. More specifically, as defined in Fig. 2(b), ΔV_h is the difference between the reverse and forward V_g values at the average of the forward and reverse V_g -sweep currents at $V_g = 0$ V.

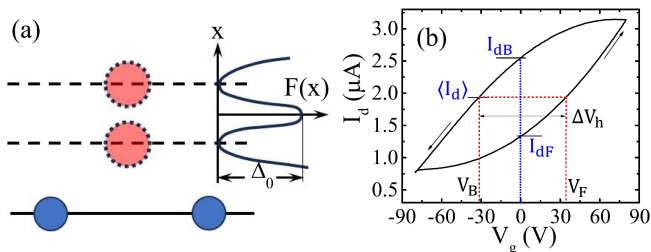


FIG. 2: The schematic (a) depicts the two minimum free-energy [$F(x)$] states of the puckered oxygen ions (red spheres) at the STO surface with large and small displacements (x) from the positively charged Sr/Ti ions (blue spheres). A negative V_g lowers the energy of the state with large displacement having larger inward dipole-moment than the other state. (b) shows the measured V_g -dependence of I_d for the MoS₂/STO FET at $V_d = 1$ V over a V_g cycle between -80 and 80 V. I_{dF} and I_{dB} are the drain currents at $V_g = 0$ during forward and backward V_g -sweeps, respectively. $\Delta V_h = V_B - V_F$ with V_F and V_B as the V_g values at $I_d = (I_{dF} + I_{dB})/2$ for the respective V_g -sweep directions.

Such counterclockwise hysteresis is commonly attributed to the ferroelectric (FE) properties of the gate material. In an n-FET with FE gate, a positive V_g amounts to an electric field pointing towards the channel leading to FE dipoles' alignment parallel to the field. Now when V_g is made zero, a FE remnant state would persist with a polarization pointing towards the channel. In such zero electric field state, the channel will acquire a negative charge density and the gate electrode will have an equal magnitude positive charge density. This to nullify the electric field in the FE due to the remnant polarization. This amounts to electron accumulation in

the n-FET channel leading to enhanced conductance and a reduced threshold V_g as compared to the zero polarization state of the FE. Similarly, when one arrives at $V_g = 0$ state from a negative V_g , there will be depletion of channel electrons resulting into loss in channel conductance and an increase of the threshold V_g . This is consistent with the counterclockwise hysteresis observed in Fig. 2(b).

STO is actually a paraelectric down to $T = 0$ K [28–31] with an inclination towards a ferroelectric transition as the temperature approaches 0 K but in the bulk there is no ferroelectricity in STO at non-zero temperatures. However, the surface atoms experience different boundary conditions and bonding environments compared to the bulk. Modifications in atomic force constants and changed phonon characteristics at the surface may induce a FE reconstruction near the surface at finite temperatures. Observation of second harmonic generation [32] shows an inversion symmetry breaking, implying dipoles on the surface of reduced STO. Some loss of oxygen at the exposed surface of an untreated STO cannot be ruled out although extremely sensitive probes may be needed to actually establish it. Further, the theory-experiment correlations suggest that the surface comprises of domains with two distinct layer-terminations. One termination features an oxygen and a strontium atoms per unit cell, *i.e.* O-Sr, referred to as “Sr termination”. The other features two oxygen and one titanium atoms per unit cell, *i.e.* O-Ti-O, referred to as “Ti termination” [38]. In both terminations, the oxygen atoms get pulled out, or displaced, from the surface under simultaneous multilayer relaxations [38–41]. This phenomenon, known as “puckering”, leads to the formation of a static inward dipole moment on the STO surface. Consequently, a thin surface layer can exhibit permanent dipole moments or a ferroelectric-like state. Such displacement will also couple to the electric field.

We believe that this FE-like counterclockwise hysteresis in the MoS₂-STO FETs arises from the response, or the dynamics, of the STO-surface oxygen-ion displacement to the gate electric field. Presence of electric field near STO surface will promote displacement of puckered oxygen ions in a direction opposite to the field which increases the dipole moment parallel to the field. This is similar to the FE polarization. Further, from the observed blocking transition, discussed later, such surface dipoles seem to exhibit a bistable behavior. This can arise from two local minima in the energy with respect to the puckered oxygen-ion displacement with an energy barrier between the two, see Fig. 2(a). From the sharpness of the blocking transition, it appears that there is a very narrow distribution of barrier energies at play. The applied gate electric-field provides a bias and lowers the energy of one of the two minima. A similar polarization may also occur at the other STO surface, close to the gate electrode, with the bulk of the STO still behaving

as a dielectric. The electric field at the STO surface for a fixed V_g will depend on the dielectric constant of the bulk STO, which has a significant temperature dependence.

Figure 3(a) shows the measured $I_d - V_g$ curves for different V_g sweep ranges varying from ± 10 ($\Delta V_g = 20$ V) to ± 80 V ($\Delta V_g = 160$ V) but at a fixed V_g sweep rate of 1.15 V/s. The hysteresis, quantified by ΔV_h increases monotonically with increasing sweep range ΔV_g , see Fig. 3(b). This happens as more oxygen-ions change their displacement in response to larger V_g sweep. As a result the I_g response also rises. A non-zero V_g acts as a bias leading to a tilt of the bistable potential, see Fig. 2(a), and with the tilt proportional to V_g . Figure 3(c) shows

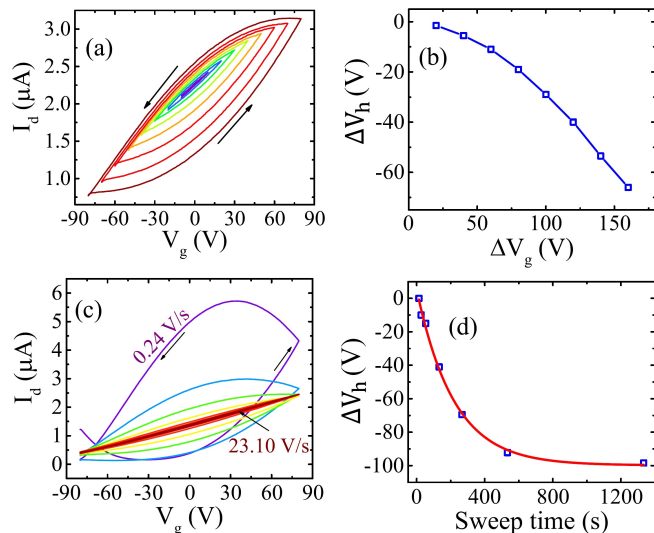


FIG. 3: (a) Room temperature $I_d - V_g$ characteristics at $V_d = 1$ V for different sweep ranges of V_g from ± 10 to ± 80 V at a constant sweep rate of 1.15 V/s. (b) shows the variation of hysteresis width ΔV_h with ΔV_g . (c) Room temperature $I_d - V_g$ curves for different sweep rates, between 0.24 and 23.1 V/s, of V_g at a fixed $V_d = 1$ V and $\Delta V_g = 160$ V. (d) shows ΔV_h as a function of total sweep time with the red line showing a fit to a single exponential relaxation with 218 s characteristic time.

the $I_d - V_g$ hysteresis loops acquired at different V_g sweep rates from 0.24 to 23.1 V/s at room temperature for fixed V_g -range. Both the hysteresis and the change in I_d are seen to reduce with increasing rate. Fig. 3(d) shows the dependence of ΔV_h on the overall sweep-time which is inversely related to sweep rate. ΔV_h is found to fit well to an exponential with a characteristic time $\tau_c = 218$ s. The sweep-range and sweep-rate dependence can be understood from earlier discussion on Blocking transition as the switching rates between the two states will increase with the increase in bias, provided by V_g , while a smaller sweep rate will enable more transitions for a fixed switching rate of the dipoles.

Figure 4(a,b) display $I_d - V_g$ curves at $V_d = 1$ V for temperatures ranging from 80 K to 390 K, over a V_g

sweep range of $\Delta V_g = 160$ V at 1.15 V/s sweep rate. The device was first kept at room temperature with $V_g = 0$ V for over 10 hours to equilibrate and then cooled to 80 K at this gate and then data were acquired after stabilizing different temperatures during the heating and up to 390 K. No difference between cooling and heating runs was found as long as V_g was kept at zero during temperature change. The counterclockwise hysteresis observed at room temperature decreases and vanishes with cooling, see Fig. 4(a). In fact, the very small hysteresis at low temperatures has an opposite sense, similar to that due to traps, as compared to the one at high temperatures. This could be due to traps either at the MoS_2/STO interface or in the bulk of MoS_2 . The hysteresis, on the other hand, increases with heating above room temperature and peaks near 350 K before decreasing. This can be seen more clearly from the temperature variation of ΔV_h in Fig. 4(c).

It can also be seen that the overall I_d -response to V_g , representing the transconductance, rises monotonically with increasing temperature above the room temperature, which is in contrast with the non-monotonic behavior of the hysteresis. Since the dielectric constant of bulk STO decreases monotonically with rising temperature one would rather expect a minor reduction in transconductance with rising temperature. From this we infer that the channel's carrier density due to the surface dipoles dominates, at least above the room temperature, over that due to the bulk dielectric polarization of STO. With cooling below room temperature, the response-time of the surface dipoles, to the V_g -change, grows and becomes much larger than the V_g sweep time. This makes the hysteresis vanish and the contribution of surface dipoles to the transconductance will also vanish. With increasing temperature the response time decreases which makes the transconductance increase as more surface dipoles respond to the V_g change. The hysteresis peaks at T_B where the response-time and the V_g sweep-time match. Well above T_B nearly all dipoles respond fast and to both, the forward and reverse, sweeps of V_g . This reduces the hysteresis but increases the transconductance further.

The hysteresis and the blocking transition can be modeled using a bistable system, discussed earlier, for surface dipoles with two energy-minima separated by a barrier Δ_0 with a bias energy E_B proportional to V_g . The continuous line in Fig. 4(c) shows a temperature dependent ΔV_h calculated using Eq. 1 with a single barrier energy Δ_0 and an energy bias E_B proportional to V_g . The parameters used for this calculated curve are $\tau_m/\tau_0 = 6 \times 10^{14}$, $\Delta_0 = 1$ eV, $aE_{B0} = bE_{B0} = 0.09$ eV at $V_g = 80$ V. The simple model of blocking transition using a bistable system captures the ΔV_h variation remarkably well.

It is found that the hysteresis together with the blocking transition and the transition temperature is nearly the same in several different studied devices, see

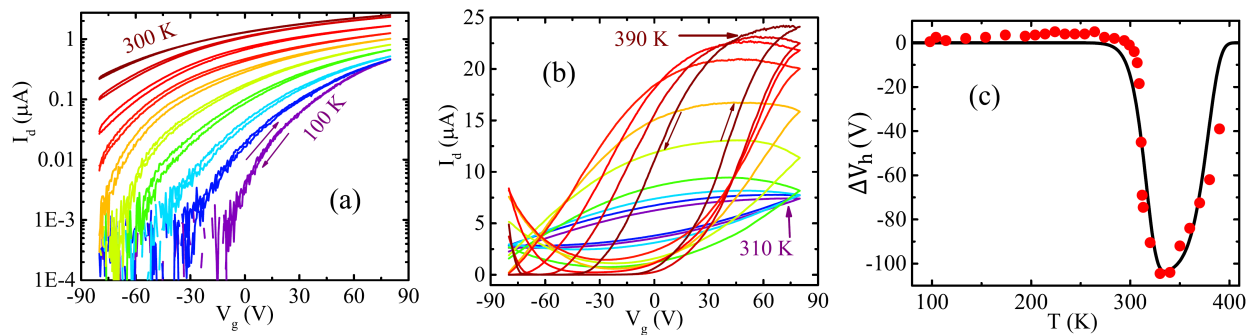


FIG. 4: (a) $I_d - V_g$ curves at $V_d = 1\text{V}$ and 1.15 V/s sweep rate for different temperatures between 100 and 300 K and (b) between 310 and 390 K. (c) Variation of ΔV_h with temperatures as found from the curves of (a) and (b) with the continuous line as the curve calculated using Eq. 1 (see text for details).

Appendix, with varying number of MoS_2 layers and MoS_2/STO interface. Although the behavior of transconductance below the room temperature somewhat varies between the samples. This could arise from the variation in defect density in MoS_2 that can lead to variation in the amount of n-doping together with a rising dielectric constant of STO with cooling. A higher n-doping can lead to larger transconductance assisted by a rising dielectric constant of STO with cooling. This is the case with one of the samples as discussed the Appendix. Anyhow, the surface dipoles' response to V_g is expected to diminish with cooling and it is independent of the contribution from other sources such as dopants and the dielectric polarization in the gate.

Although the underlying blocking physics here is similar to that of the interface traps [13] but there are some crucial differences. The activation of traps in response to the gate electric field leads to screening of the electric field seen by the channel while the surface dipoles enhance the field. Thus, in the case of interface traps the sense of hysteresis is opposite, *i.e.* clockwise, and the increasing traps' participation with rising temperature reduces the transconductance or I_d change with V_g . Further, the hysteresis keeps rising with temperature in case of traps with a steep rise at a particular temperature but in case of surface dipoles the hysteresis exhibits a clear peak. This is due to a wide distribution in barrier energy in case of traps but the surface dipoles appear to have a very narrow distribution in barrier energy. This implies a much less disordered nature of surface dipoles in STO than the traps.

Figure 5(a) shows the I_d relaxations at different temperatures when V_g is abruptly switched from -80 to 80 V at $t = 0\text{ s}$. V_g was held at -80 V for more than 3 hours to achieve near equilibrium conditions with the MoS_2 channel in the off state. At $t = 0$, when the V_g is abruptly changed, there is a tiny jump in I_d followed by a relatively slow rise. The abrupt jump is attributed to the bulk STO dielectric induced channel carriers while the slow rise is due to the surface dipoles. With increas-

ing temperatures the time associated with the slow rise decreases monotonically while below room temperature this time is extremely large. Fig. 5(b) shows the I_d re-

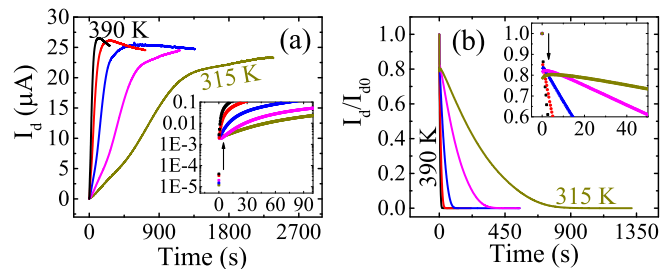


FIG. 5: (a) Time-dependence of I_d at $T = 315, 330, 350, 370$ and 390 K temperatures when V_g is changed from -80 to 80 V at $t = 0\text{ s}$. The inset shows the zoomed-in portion of the graph with the arrow indicating the sudden jump in I_d at $t = 0$. (b) Time-dependence of I_d at $T = 315, 330, 350, 370$ and 390 K when V_g is stepped from 80 V to -80 V at $t = 0\text{ s}$. The inset shows the zoomed-in portion with the arrow indicating the sudden jump at $t = 0$. In (b), the vertical axis has been normalized with I_{d0} of respective temperatures. I_{d0} is the current at $V_g = 80\text{ V}$ and just before the voltage step.

laxation, scaled with the respective saturated values at 80 V , as a function of time when the V_g is changed from 80 to -80 V at $t = 0\text{ s}$. There is a small abrupt downward jump in I_d due to STO dielectric response, see Fig. 5(b) inset, followed by a slow decrease due to surface dipoles' response. In both cases, such activated response time behavior is consistent with the two state model discussed earlier.

Figure 6(a) shows the effect of cooling on the $I_d - V_g$ curves measured at 80 K when the device is cooled from 350 to 80 K under different gate-cooling voltages V_{gc} from -80 V to 80 V . For each V_{gc} , the device was kept at 350 K in vacuum at the desired V_{gc} for one hour and then cooled to 80 K in its presence. As expected, there is negligible hysteresis at 80 K , but a significant shift in the threshold voltage V_{th} ranging between -78 and $+60\text{ V}$, depending on the V_{gc} value. Fig. 6(b) shows the monotonic decrease

of V_{th} with V_{gc} . This is easily expected from the block-

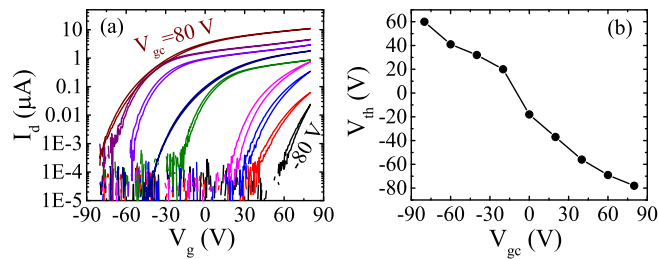


FIG. 6: (a) shows the $I_d - V_g$ curves at $V_d = 1$ V and at 80 K after cooling the FET from 350 to 80 K under different applied gate voltages V_{gc} from -80 V to 80 V in steps of 20 V. (b) shows the variation of threshold-voltage V_{th} with V_{gc} .

ing transition that happens near 350 K above which the surface dipoles are unblocked and respond fast to the V_g change. When gate-cooled, the dipoles get blocked in the changed configuration the dipoles freeze or get blocked again. This enables a reversible control on V_{th} . For negative V_{gc} , the surface dipoles exhibit a dipole moment pointing away from the channel as compared to zero V_{gc} . This depletes electrons from the MoS₂ channel and leads to an increase in V_{th} . In contrast, the positive V_{gc} leads to a decrease in V_{th} . Thus, the STO surface dipoles act as a virtual gate, enabling heat-assisted non-volatile memory.

DISCUSSIONS AND CONCLUSIONS

In a superparamagnet, the magnetic field needed to make the potential monostable is experimentally accessible. As a result, for such large fields the hysteresis is seen at low temperatures but it vanishes at high temperatures and above the blocking transition in contrast with the surface dipoles as well as the interface traps. The field required to make the potential monostable for traps can easily be higher than the breakdown field of the gate material. However, in case of STO surface dipoles, it will be interesting to see if sufficiently large gate electric field is achievable to make the potential monostable. This can have useful consequences for using these surface dipoles in memory applications. It's also noteworthy that MoS₂ acts as a sensitive detector of such small ionic displacements.

The counterclockwise hysteresis due to surface dipoles could not be eliminated by a HMDS passivation layer, see Appendix, as opposed to the interface traps [13] where the passivation layer blocks the transfer of charge between the channel and the traps. Thus the presence of HMDS or the roughness, see Appendix, of the STO surface do not eliminate the hysteresis and the blocking transition. Sachs et. al. [25] found similar counterclockwise hysteresis in graphene-STO FETs at room temperature which vanished with cooling but without any hysteresis

in the Au/STO/Au parallel-plate capacitors ruling out ferroelectricity in the bulk STO. A deposited metal layer on STO could alter the surface dipole layer to eliminate their field response while the 2D layer of graphene or MoS₂ does not bond enough to alter the surface dipoles.

In conclusion, a blocking transition near 350 K resulting from the bistable surface dipoles in STO is found and studied systematically in MoS₂/STO FET devices. This transition occurs when the activated transition rate, arising from the interplay of thermal energy and a barrier-energy between two states, matches with the gate-voltage sweep-rate. A peak in counterclockwise hysteresis and rising transconductance above room temperature is thus observed. The blocking is used to demonstrate an interesting memory effect of the surface dipoles enabling a control on the FET's threshold voltage at low temperatures which has application potential in non-volatile memory. This also illustrates MoS₂ as a sensitive detector of surface polarization.

ACKNOWLEDGMENTS

The authors acknowledge funding from the SERB-DST of the Government of India and from IIT Kanpur.

APPENDIX: ADDITIONAL DATA ON DEVICES WITH DIFFERENT INTERFACES

Two additional multilayer MoS₂/STO FET devices were studied with different interfaces to verify the reproducibility of the counterclockwise hysteresis and the blocking transition of STO surface dipoles in such devices.

Figures 7(a,b) show the $I_d - V_g$ curves of an MoS₂/STO FET without HMDS passivation on the STO surface. This was measured at $V_d = 1$ V over a temperature range from 80 K to 390 K, using the same V_g sweep range and rate as described in the main paper. Figs. 7(d,e) show the same for an MoS₂ FET prepared on the rough surface of STO and with HMDS passivation and over a temperature range from 80 K to 395 K. Both these samples display a counterclockwise hysteresis at room temperature, which decreases sharply and vanishes upon cooling, as shown in Fig. 7(a) and (d). Upon heating, the hysteresis increases and peaks around 350 K before decreasing again, see Figs. 7(c) and (f). This latter sample indicates that surface roughness did not alter the polarization dynamics at the MoS₂-STO interface. This result contrasts with previous work on PZT-gated MoS₂ FETs [16], where surface roughness changed the hysteresis direction from anticlockwise to clockwise due to the interface states induced by defects on the rough surface. The below room temperature behavior of the three studied devices has differences as elaborated earlier but the blocking transition

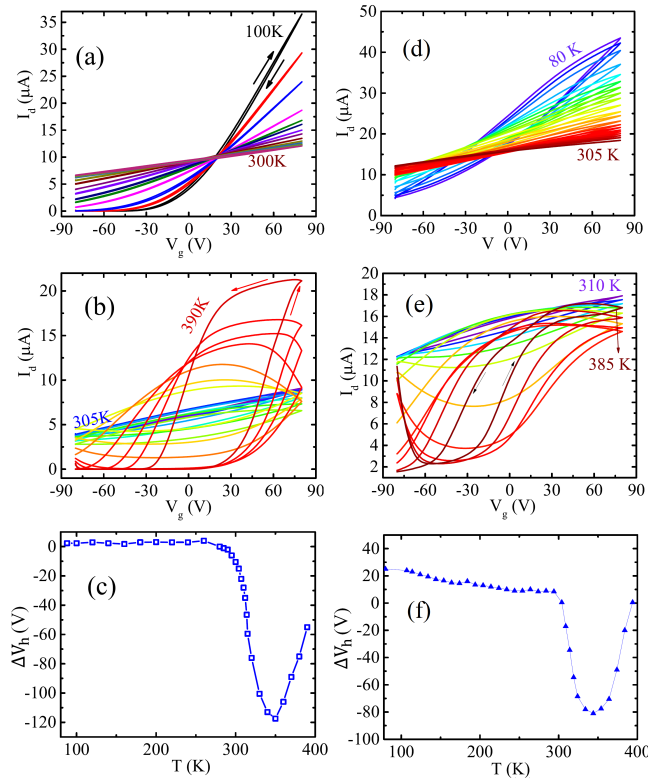


FIG. 7: (a) $I_d - V_g$ curves for different temperatures between 100 K and 300 K and (b) between 305 K and 390 K at $V_d = 1\text{V}$. (c) ΔV at different temperatures extracted from the curves of (a) and (b). (d) $I_d - V_g$ curves for different temperatures between 80 K and 305 K and (e) between 310 K and 385 K at $V_d = 1\text{V}$. (f) ΔV at different temperatures extracted from the curves of (d) and (e).

and the clockwise hysteresis above room temperature in all three studied devices are nearly the same.

REFERENCES

- [1] Z. Zhou, and Y. K. Yap, “Two-dimensional electronics and optoelectronics: present and future Electronics”, *Electronics* **6**, 53 (2017).
- [2] K. F. Mak, C. Lee, J. Hone, J. Shan, and T. F. Heinz, “Atomically thin MoS_2 : a new direct-gap semiconductor”, *Phys. Rev. Lett.* **105**, 136805 (2010).
- [3] B. Radisavljevic, A. Radenovic, J. Brivio, V. Giacometti, and A. Kis, “Single-Layer MoS_2 Transistors”, *Nat. Nanotechnol.* **6**, 147 (2011).
- [4] L. M. Martinez, N. J. Pinto, C. H. Naylor, and A. T. Johnson, “ MoS_2 based dual input logic AND gate”, *AIP Adv.* **6**, 125041 (2016).
- [5] S. Wachter, D. K. Polyushkin, O. Bethge, and T. Mueller, “A microprocessor based on a two-dimensional semiconductor”, *Nat. Commun.* **8**, 14948 (2017).
- [6] D. Krasnozhan, D. Lembke, C. Nyffeler, Y. Leblebici, and A. Kis, “ MoS_2 Transistors Operating at Gigahertz Frequencies”, *Nano Lett.* **14**(10), 5905 (2014).
- [7] O. L. Sanchez, D. Lembke, M. Kayci, A. Radenovic, and A. Kis, “Ultrasensitive photodetectors based on monolayer MoS_2 ”, *Nat. Nanotechnol.* **8**, 497 (2013).
- [8] O. L. Sanchez, E. A. Llado, V. Koman, A. F. Morral, A. Radenovic, and A. Kis, “Light generation and harvesting in a van der Waals heterostructure”, *ACS Nano* **8**, 3042 (2014).
- [9] M. L. Tsai, S. H. Su, J. K. Chang, D. S. Tsai, C. H. Chen, C. I. Wu, L. J. Li, L. J. Chen, and J. H. He, “Mono-layer MoS_2 heterojunction solar cells”, *ACS Nano* **8**(8), 8317 (2014).
- [10] D. J. Late, B. Liu, H. S. S. R. Matte, V. P. Dravid, and C. N. R. Rao, “Hysteresis in Single-Layer MoS_2 Field Effect Transistors”, *ACS Nano* **6**(6), 5635 (2012).
- [11] Y. Park, H. W. Baac, J. Heo, and G. Yoo, “Thermally activated trap charges responsible for hysteresis in multilayer MoS_2 field-effect transistors”, *Appl. Phys. Lett.* **108**, 083102 (2016).
- [12] Y. Y. Illarionov, G. Rzepa, M. Waltl, T. Knobloch, A. Grill, M. M. Furchi, T. Mueller, and T. Grasser, “The role of charge trapping in $\text{MoS}_2/\text{SiO}_2$ and MoS_2/hBN field-effect transistors”, *2D Mater.* **3**, 035004 (2016).
- [13] S. P. Jana, S. Gupta, and A. K. Gupta, “Blocking transition of interface traps in $\text{MoS}_2/\text{SiO}_2$ field-effect transistors”, *Phys. Rev. B* **108**, 195411 (2023).
- [14] N. Mohta, R. K. Mech, S. Sanjay, R. Muralidharan, and D. N. Nath, “Artificial Synapse Based on Back-Gated MoS_2 Field-Effect Transistor with High-k Ta_2O_5 Dielectrics”, *Phys. Status Solidi A* **217**, 2000254 (2020).
- [15] T. Li, L. Gao, H. Xie, L. Ye, W. Yang, Q. Liu, and K. Li, “Intrinsic counterclockwise hysteresis in Mn-doped $\text{Pb}(\text{Zr},\text{Ti})\text{O}_3$ gated MoS_2 field effect transistors”, *Mater. Res. Express* **5**(6), 066308 (2018).
- [16] Z. Lu, C. Serrao, A. I. Khan, L. You, J. C. Wong, Y. Ye, H. Zhu, X. Zhang, and S. Salahuddin, “Nonvolatile MoS_2 field effect transistors directly gated by single crystalline epitaxial ferroelectric”, *Appl. Phys. Lett.* **111**(2), 022902 (2017).
- [17] K. L. Ganapathi, M. Rath, and M. S. R. Rao, “Polarization induced switching in PZT back gated multilayer MoS_2 FETs for low power non-volatile memory”, *Semicond. Sci. Technol.* **34**, 055016 (2019).
- [18] A. Lipatov, P. Sharma, A. Gruverman, and A. Sinitiskii, “Optoelectrical Molybdenum Disulfide (MoS_2) Ferroelectric Memories”, *ACS Nano* **9**, 8089 (2015).
- [19] X.-W. Zhang, D. Xie, J.-L. Xu, Y.-L. Sun, X. Li, C. Zhang, and R.-X. Dai, “ MoS_2 field-effect transistors with lead zirconate-titanate ferroelectric gating”, *IEEE Electron Device Lett.* **36**, 784 (2015).
- [20] C. Zhou, X. Wang, S. Raju, Z. Lin, D. Villaroman, B. Huang, and Y. Chai, “Low voltage and high ON/OFF ratio field-effect transistors based on CVD MoS_2 and ultra high-k gate dielectric PZT”, *Nanoscale* **7**, 8695 (2015).
- [21] T. Sakudo, and H. Unoki, “Dielectric Properties of SrTiO_3 at Low Temperatures”, *Phys. Rev. Lett.* **26**, 851 (1971).
- [22] S. Saha, O. Kahya, M. Jaiswal, A. Srivastava, A. Annadi, J. Balakrishnan, A. Pachoud, C.-T. Toh, B.-H. Hong, J.-H. Ahn, T. Venkatesan, and B. Ozyilmaz, “Unconventional Transport Through Graphene on SrTiO_3 : A

- Plausible Effect of SrTiO₃ Phase-Transitions”, *Sci. Rep.* **4**, 6173 (2015).
- [23] K. T. Kang, H. Kang, J. Park, D. Suh, and W. S. Choi, “Quantum Conductance Probing of Oxygen Vacancies in SrTiO₃ Epitaxial Thin Film Using Graphene”, *Adv. Mater.* **29**, 1700071 (2017).
- [24] N. J. G. Couto, B. Sacepe, and A. F. Morpurgo, “Transport Through Graphene on SrTiO₃”, *Phys. Rev. Lett.* **107**, 1-5 (2011).
- [25] R. Sachs, Z. Lin, and J. Shi, “Ferroelectric-Like SrTiO₃ Surface Dipoles Probed by Graphene”, *Sci. Rep.* **4**, No. 3657 (2014).
- [26] A. Sahoo, D. Nafday, T. Paul, R. Ruiter, A. Roy, M. Mostovoy, T. Banerjee, T. Saha-Dasgupta, and A. Ghosh, “Out-of-Plane Interface Dipoles and Anti-Hysteresis in Graphene-Strontium Titanate Hybrid Transistor”, *npj 2D Mater. Appl.* **2**, No. 9 (2018).
- [27] S. Chen, X. Chen, E. A. Duijnste, B. Sanyal, and T. Banerjee, “Unveiling temperature-induced structural domains and movement of oxygen vacancies in SrTiO₃ with graphene”, *ACS Appl. Mater. Interfaces* **12**, 52915-52921 (2020).
- [28] A. D. Bruce, and R. A. Cowley, “Lattice dynamics of strontium titanate: anharmonic interactions and structural phase transitions”, *J. Phys. C: Solid State Phys.* **6**, 2422 (1973).
- [29] R. Migoni, H. Bilz, and D. Bäuerle, “Origin of Raman scattering and ferroelectricity in oxidic perovskites”, *Phys. Rev. Lett.* **37**, 1155 (1976).
- [30] S. E. Rowley, L. J. Spalek, R. P. Smith, M. P. M. Dean, M. Itoh, J. F. Scott, G. G. Lonzarich, and S. S. Saxena, “Ferroelectric quantum criticality”, *Nat. Phys.* **10**, 367-372 (2014).
- [31] A. Müller, and H. Burkard, “SrTiO₃: An intrinsic quantum paraelectric below 4 K”, *Phys. Rev. B* **19**, 3593 (1979).
- [32] B. Kang, “Second-harmonic Generation of Treated-STO Surface”, *J. Kor. Cer. Soc.*, **49**, 142 (2012).
- [33] A. C. Gomez, M. Buscema, R. Molenaar, V. Singh, L. Janssen, H. S. Van Der Zant, and G. A. Steele, “Deterministic transfer of two-dimensional materials by all-dry viscoelastic stamping”, *2D Mater.* **1**, 011002 (2014).
- [34] S. P. Jana, S. Shivangi, S. Gupta, and A. K. Gupta, “Enhanced performance of MoS₂/SiO₂ field-effect transistors by hexamethyldisilazane (HMDS) encapsulation”, *Appl. Phys. Lett.* **124**, 241101 (2024).
- [35] P. Chen, W. Xu, Y. Gao, J. H. Warner, and M. R. Castell, “Epitaxial Growth of Monolayer MoS₂ on SrTiO₃ Single Crystal Substrates for Applications in Nanoelectronics”, *ACS Appl. Nano Mater.* **1**, 6976-6988 (2018).
- [36] C. Lee, H. Yan, L. E. Brus, T. F. Heinz, J. Hone, and S. Ryu, “Anomalous Lattice Vibrations of Single and Few-Layer MoS₂”, *ACS Nano* **4**(5), 2695 (2010).
- [37] J. Petzelt, T. Ostapchuk, I. Gregora, I. Rychetský, S. Hoffmann-Eifert, A. V. Pronin, Y. Yuzyuk, B. P. Gorshunov, S. Kamba, V. Bovtun, and J. Pokorný, “Dielectric, infrared, and Raman response of undoped SrTiO₃ ceramics: Evidence of polar grain boundaries”, *Phys. Rev. B* **64**, 184111 (2001).
- [38] N. Bickel, G. Schmidt, K. Heinz, and K. Müller, “Ferroelectric relaxation of the SrTiO₃ (100) surface”, *Phys. Rev. Lett.* **62**, 2009 (1989).
- [39] J. Hanzig, M. Zschornak, F. Hanzig, E. Mehner, H. Stöcker, B. Abendroth, C. Röder, A. Talkenberger, G. Schreiber, D. Rafaja, and S. Gemming, “Migration-induced field-stabilized polar phase in strontium titanate single crystals at room temperature”, *Phys. Rev. B Condens. Matter Mater. Phys.* **88**, 024104 (2013).
- [40] T. Leisegang, H. Stöcker, A. A. Levin, T. Weißbach, M. Zschornak, E. Gutmann, K. Rickers, S. Gemming, and D. C. Meyer, “Switching Ti valence in SrTiO₃ by a dc electric field”, *Phys. Rev. Lett.* **102**, 087601 (2009).
- [41] E. Heifets, E. A. Kotomin, and J. Maier, “Semi-empirical simulations of surface relaxation for perovskite titanates”, *Surf. Sci.* **462**, 19-35 (2000).
- [42] A. K. Singh, and A. K. Gupta, “Reversible control of doping in graphene-on-SiO₂ by cooling under gate-voltage”, *J. Appl. Phys.* **122**, 195305 (2017).